Molecular Crystals and Liquid Crystals

ISSN: 1542-1406 (Print) 1563-5287 (Online) Journal homepage: http://www.tandfonline.com/loi/gmcl20

Electrical Measurements on P3HT:CdSe Blends for Photovoltaic Applications

V. Kažukauskas, A. Sakavičius, E. Couderc, V. Janonis, P. Reiss, D. Djurado & J. Faure-Vincent

To cite this article: V. Kažukauskas, A. Sakavičius, E. Couderc, V. Janonis, P. Reiss, D. Djurado & J. Faure-Vincent (2014) Electrical Measurements on P3HT:CdSe Blends for Photovoltaic Applications, Molecular Crystals and Liquid Crystals, 604:1, 174-183, DOI: 10.1080/15421406.2014.968485

To link to this article: http://dx.doi.org/10.1080/15421406.2014.968485

Published online: 15 Dec 2014.

Mol. Cryst. Liq. Cryst., Vol. 604: pp. 174–183, 2014

ISSN: 1542-1406 print/1563-5287 online
DOI: 10.1080/15421406.2014.968485

Electrical Measurements on P3HT:CdSe Blends for Photovoltaic Applications

V. KAŽUKAUSKAS,[1,*] A. SAKAVIČIUS,[1] E. COUDERC,[2,3] V. JANONIS,[1] P. REISS,[2] D. DJURADO,[2] AND J. FAURE-VINCENT[2]

[1]Semiconductor Physics Department and Institute of Applied Research, Vilnius University, Vilnius, Lithuania
[2]SPrAM Laboratory, UMR CEA-CNRS-University of Grenoble, Grenoble, France
[3]Center for Energy Nanoscience and Department of Chemistry, University of Southern California, Los Angeles, USA

Hybrid photovoltaic structures made of P3HT and branched CdSe nanocrystals (NCs) with 50 wt%–90 wt% ratio were investigated. Charge Extraction by Linearly Increasing Voltage (CELIV) mobility and temperature dependent (photo-)conductivity measurements were used to analyze the charge transport. The samples with 50 wt% were photosensitive, but just a minor PV effect was observed. The photovoltaic phenomenon was pronounced in the samples containing 75 wt% or more of NCs. The Open Circuit Voltages up to 1 V were obtained. The recombination of the generated carriers was fast and could be a limiting factor of the cell current. Carrier mobility was up to (3−4) × 10^{-4} cm^2/Vs. From the fitting of mobility data the best carrier transport conditions were found in the samples with 75 wt% and 83 wt% of NCs.

Keywords P3HT; CdSe; nanocrystals; hybrid solar cells; mobility; charge transport

Introduction

Blends composed of organic polymers and inorganic nanocrystals are of high interest in the field of photovoltaic cells. Hybrid organic/inorganic photovoltaic cells comprise of an organic matrix with inorganic nanocrystals (NCs), which behave as electron acceptors in bulk heterojunction structure. These hybrid material systems have indeed several advantages as, e.g., solution phase processing, flexibility, their shape can be varied, enabling tuning of the percolation threshold, their HOMO and LUMO levels can also be varied, tuning the absorption spectrum [1]. Notable energy conversion efficiencies (η) up to 4.1% have been reached recently on P3HT:CdS [2] based solar cells. Other promising results have been obtained with CdSe nanocrystals mixed with different

*Address correspondence to V. Kažukauskas, Semiconductor Physics Department and Institute of Applied Research, Vilnius University, Saulėtekio al. 9, bldg. 3, LT-10222 Vilnius, Lithuania; E-mail: vaidotas.kazukauskas@ff.vu.lt

Color versions of one or more of the figures in the article can be found online at www.tandfonline.com/gmcl.

conjugated polymers like poly[2,6-(4,4-bis(2-ethylhexyl)-4H-cyclopenta[2,1-b;3,4-b′]-dithiophene)-alt-4,7-(2,1,3-benzothiadiazole) (PCPDTBT) ($\eta = 4.7\%$) [3], poly[2,5 thiophen-2-yl)thieno[3,2-b]thiophene and thieno[3,4-c]pyrrole-4,6-dione] (PDTTTPD) ($\eta = 2.9\%$) [4] or P3HT ($\eta = 2.7\%$) [5]. However, the efficiency of such systems remains low compared to that obtained with the same polymers blended with PCBM ([6,6]-phenyl-C_{61}-butyric acid methyl ester) instead of nanocrystals (e.g., 5% for PCPDTBT [6], 5.1% for PDTTTPD [7], 5% for P3HT [8]). This difference in efficiencies points out that the concepts derived from polymer:PCBM blends are not easily transposable to organic/inorganic hybrids and that our understanding of these hybrid systems has still to be improved. In the case of P3HT:CdSe blends, the solar cell efficiency has been proved to be slightly enhanced by using branched NCs (e.g. tetrapods) instead of nanodots [5, 9]. This is due to a better electrical connectivity between the branched NCs leading to more efficient charge collection within the active layer [10].

In this paper, we focused on the electrical properties of hybrid blends made of P3HT and branched CdSe NCs. To evaluate the impact of the NCs content in the blend on the device performance and its origins in the charge transport mechanism, we screened different weight proportions from 50 wt% (16 vol%) to 90 wt% (63 vol%). We utilized the Charge Extraction by Linear Increasing Voltage (CELIV) and temperature dependent conductivity measurements to analyze the charge mobility, energetical and positional disorder parameters, and activation energy.

Synthesis and Experimental

The poly(3-hexylthiophene) (P3HT) (from Merck) was fractioned and its characteristics are $M_n = 28.5$ kDa, $M_w = 46.4$ kDa, PDI = 1.63, regioregularity index 95.9%. The solution of P3HT was prepared in chloroform ($CHCl_3$) at a concentration of 15 mg/mL. The CdSe NCs synthesis is described in [11]. To obtain branched nanostructures, the synthesis was adapted by using a lower injection temperature. Trioctylphosphine (TOP, 200 mL) and selenium powder (0.08 mol) were mixed in a flask in the glovebox and stirred overnight to obtain 200 mL of TOP-Se at 0.4 M. Cadmium stearate (8 mmol), stearic acid (184 mmol), oleylamine (280 mL) and octadecene (186 mL) were introduced into the 2 L reactor, degazed for one hour and finally put under argon atmosphere. The mixture was then heated to 230°C and mechanically stirred. When the reaction temperature was reached, 200 mL of TOP-Se were rapidly injected by means of a peristaltic pump and the injection tail was stopped rapidly by closing a valve. When the temperature of the mixture reached 230°C again, the reaction was left to take place for 18 minutes. The heat was then turned off. After cooling the reaction mixture to 80°C, 500 mL of acetone were introduced, then 200 mL of ethanol when the temperature reached 70°C and finally 300 mL of acetone when the temperature reached 50°C. The NCs were precipitated by addition of methanol, and recovered by centrifugation for 25 minutes at 11 000 rpm. Finally, NCs are redispersed in hexane. The obtained NCs were branched (a mixture of bipods, tripods and tetrapods), with average arm and core diameters of 3.8 nm and average arm length of 6.3 nm. In this protocol, the temperature control is very important since if the temperature is set to 250°C, the resulting NCs have a spherical shape. For spherical NCs, energy levels were determined at −3.57 eV for the LUMO and −5.67 eV for the HOMO, so the electronic gap was 2.1 eV.

The hybrid solutions were prepared by blending the P3HT solution in $CHCl_3$ at 15 mg/mL with NC solution at the adequate concentration to obtain NC weight fractions of 90 wt%, 83 wt%, 75 wt% and 50 wt%, and stirred for 2–3 hrs at 40°C. ITO substrates were etched with aqua-regia to pattern electrodes and cleaned by successive sonications in

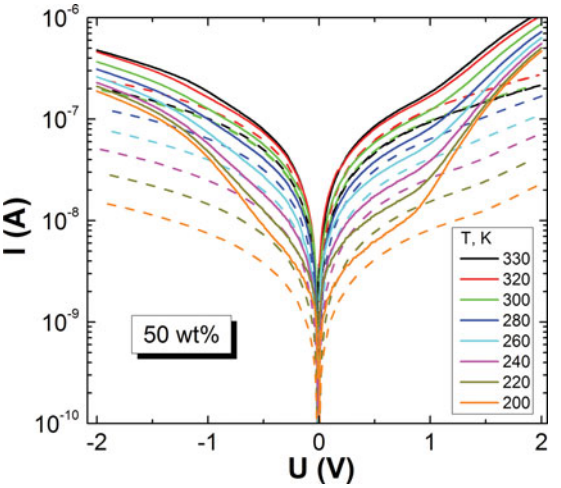

Figure 1. IVs of the sample with 50 wt% of NCs measured at different temperatures in the dark (dashed lines) and upon light illumination (solid curves).

trichloroethylene, acetone and isopropanol baths. The hybrid solutions were spun in air in 3 consecutive steps: 10 seconds at 500 rpm (acceleration 200 rpm/s), 40 seconds at 1,500 rpm (acceleration 200 rpm/s) and 60 seconds at 2,500 rpm (acceleration 200 rpm/s). Finally, samples were annealed under primary vacuum in a Büchi oven for one hour, with slow temperature ramps up to 130°C and down to room temperature. Finally, an Al cathode was evaporated (150 nm). The sample thicknesses were around 300 nm, and the electrode area was 4 mm^2.

Carrier mobility measurements were performed by the photo-CELIV (Charge Extraction by Linearly Increasing Voltage) method, Current-Voltage characterizations at different temperatures were used to investigate carrier injection and photovoltaic properties, and temperature dependent (photo-) conductivity measurements were done to evaluate the effective thermal activation energy values.

Results and Discussion

The fraction of CdSe NCs influences strongly the transport characteristics in the hybrid blends. Figures 1 and 2 show current/voltage (IV) characteristics for samples containing 50 wt% and 75 wt% of NCs, respectively.

Dark IV characteristics did not exhibit a rectifying behavior for any of the samples: IV curves are linear and symmetric at both voltage polarities. This can be explained by the high volume resistivity of the materials themselves, dominating over the contact injection in forward bias. Moreover, the dark current demonstrates a clearly thermally activated behavior, i.e., the exponential dependence of this sample volume resistance R_s on the inverse of the temperature. The thermally activated behavior could be due to the thermal generation of carriers or to the increase of the charge mobility with the temperature T:

$$R_s = R_{s0} \exp\left(\frac{eE_A}{kT}\right), \tag{1}$$

here E_A is the effective thermal activation energy value of sample resistance, and k is Boltzmann constant. In all samples these thermal activation energy values measured in the

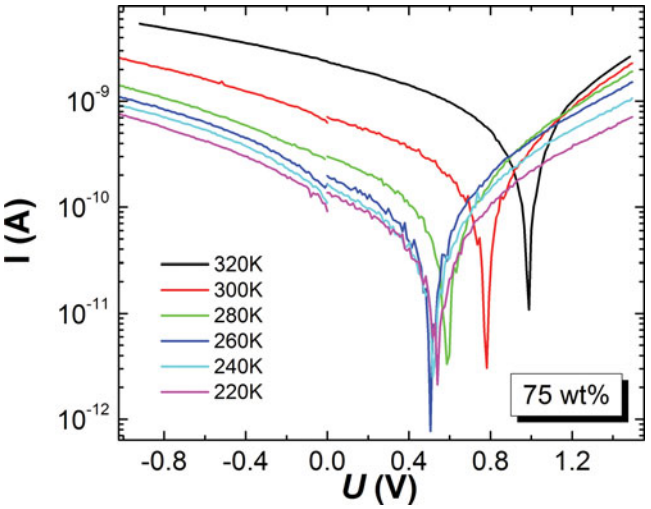

Figure 2. IVs of the sample with 75 wt% of NCs measured upon light excitation at different temperatures.

dark were very similar: 0.14–0.18 eV, the higher values being characteristic for the samples with the higher NC content (see Table 1).

The rectifying behavior above about 1 V becomes evident upon illumination (Fig. 1). Meanwhile below that value leakage current I_L is prevailing. The exponential behavior of current $I(U)$ on applied voltage U can be described by the Schottky barrier model as in [12]. This general diode equation describes the I-V characteristics of both p-n junctions and Schottky diodes:

$$I(U) = I_s \left[\exp\left(-\frac{eU - I(U)R_s}{nkT} \right) - 1 \right] + I_L, \tag{2}$$

here I_s is a saturation current, R_s is a serial resistance of the sample volume, n is the ideality factor, T is temperature, e is elementary charge. n is unity in the Shockley theory for *p-n* junctions in the absence of recombination, as well as for thermionic emission theory and diffusion theory for Schottky diodes. The ideality factor and the saturation current can be obtained from the slope and the intercept, respectively, obtained by extrapolation of the

Table 1. Thermal activation energy values of sample conductivities measured in the dark and upon light excitation in both voltage polarities

NC content in wt% – in vol%.	Dark reverse	Dark forward	Light reverse	Light forward
90–63	**0.18 eV**	**0.16 eV**	**0.38 eV**	**0.24 eV**
83–49	**0.18 eV**	**0.16 eV**	**0.33 eV**	**0.165 eV**
75–36	**0.16 eV**	**0.15 eV**	**0.22 eV**	**0.14 eV**
50–16	**0.15 eV**	**0.14 eV**	**0.102 eV**	**0.106 eV**

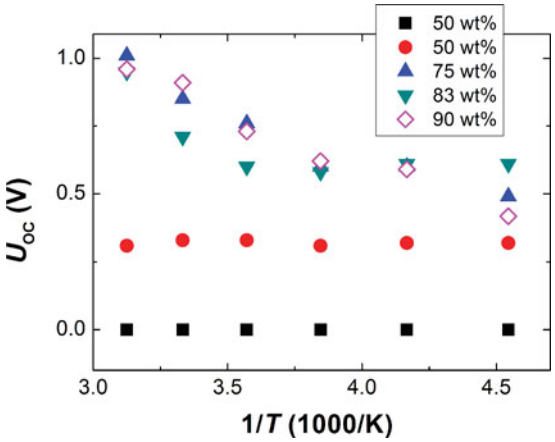

Figure 3. Temperature dependencies of V_{oc} in the samples with different content of CdSe NCs.

linear part of the semilogarithmic plot of I vs U. The saturation current density is given by:

$$j_s = A^* T^2 \exp\left(-\frac{e\Phi_B}{kT}\right), \tag{3}$$

here A^* is the Richardson constant and Φ_B is a contact potential barrier. The slow growth of the reverse current with voltage could be due to the field-assisted thermionic injection over the image force barrier (Schottky effect) [13]:

$$j = AF^{3/4} \exp\left(2\sqrt{\frac{e\gamma}{kT}F}\right), \tag{4}$$

here F is electric field, $\gamma = e^2/16\pi\varepsilon\varepsilon_0 kT$, and $A(F) = \text{const}$. Unfortunately this model, though explaining the field dependence of the reverse current, does not give any numerical values characterizing the barrier.

As mentioned before, the samples with 50 wt% of NCs were photosensitive, but their photovoltaic properties were absent or weak (see Fig. 1 or Fig. 3 respectively). This is related to the low content of NCs, as 50 wt% only corresponds to 16 vol% of NCs in the hybrid blend (as a comparison, 50 wt% of PCBM molecules corresponds roughly to 50 vol%). Hence, here, we are probing very low NC contents and the absence of photovoltaic properties is expected: the small donor-acceptor interfacial area and the lack of percolation pathways both lead to poor photo-generation of carriers and important recombination. Moreover, in 50 wt% samples, the thermal activation energy of the conductance decreased upon illumination relative to the dark activation energy (see Table 1). This is once again characteristic of the photogeneration phenomena prevailing in the sample volume rather than being caused by charge carrier injection at the contacts.

In Fig. 2, IVs of the sample with 75 wt% of NCs measured upon light excitation are presented. The photovoltaic properties are seen with high V_{OC}, but still very low currents. Similar behavior was observed for all samples with higher content of NCs. Temperature dependencies of V_{OC} in the samples with different content of CdSe NCs are presented in Fig. 3. The highest V_{oc} values were measured for the samples with 75 wt% of CdSe NCs or more. For these high NC contents samples, V_{oc} increased with increasing temperature. This observation is consistent with an efficient thermally-activated hopping transport that

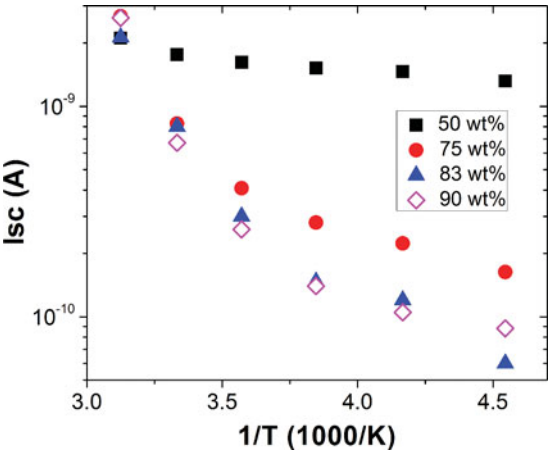

Figure 4. Temperature dependencies of I_{SC} in the samples with different content of CdSe NCs.

outcompetes recombination [14]. The growth of V_{OC} upon ageing was also observed in [15].

The photo-current at short circuit also depends on temperature, as shown in Fig. 4. Thermally-assisted carrier photo-generation becomes more important as the NC content increases. In contrast in the samples with low content of NCs at about 50 wt% upon the illumination nearly no thermal activation takes place, indicating the prevailing role of big amount of the light-generated carriers, which are screening the existing small numbers of junctions and/or potential barriers.

Altogether, Figs. 3 and 4 show that the photovoltaic characteristics are improved for higher NC contents in the hybrid blends. This is consistent with the weight ratios used in efficient hybrid devices (once again, these weight ratio are larger in hybrids than in all-organic solar cells due to the large density difference between inorganic NCs and PCBM). This also matches the optimal content of NCs determined by Time-of-Flight mobility measurements as detailed in [11].

We now turn to time-resolved measurements in order to characterize recombination and to quantify mobilities in the hybrid blends. In all samples the light-induced carrier generation and recombination was quite fast (shorter than second) even at low temperatures (Fig. 5), which is surprising, because we usually observe long-lasting (hundreds to thousands seconds) relaxation in disordered materials. It is obvious that the fast recombination of the light generated carriers diminishes charge transport. As the photoconductivity is best expressed at low temperatures we have measured its kinetics namely in the cooled samples. It can be seen from Fig. 5 that the current growth and decay are very fast. Such fast recombination prevents observation of the Thermally Stimulated Currents caused by trapped carriers, which is usually useful and informative method for studying trapping phenomena [16].

Carrier mobility dependencies in the samples were measured by the Charge Extraction by Linearly Increasing Voltage (CELIV) method depending on the electric field strength at different temperatures, as, e.g., in [17]. Examples of characteristic CELIV traces are presented in Fig. 6 at different temperatures. It can be clearly seen that at low temperatures, the extraction of the carriers takes significantly longer times (note the different time scales). This results from lower mobilities at low temperatures, consistently with the

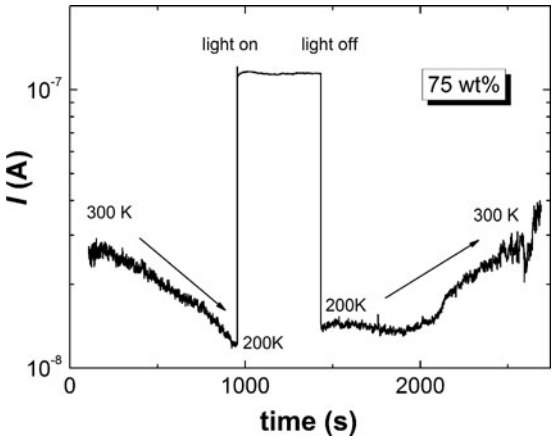

Figure 5. Current kinetics upon cooling of the sample, its light excitation and the following heating.

thermally-activated transport mechanism discussed above in the presentation of steady-state measurements. On the other hand in both cases generation of the extracted carriers during the first pulse occurs quite fast as already discussed above.

The carrier mobilities as a function of the electric field strength at different temperatures are given in Fig. 7 for the sample with 90 wt% of NCs. First, it can be seen that in the investigated sample the mobility increases with increasing temperature, as expected from the picture of thermally-activated transport. Second, the usual mobility increase with electric field prevails in contrast to the so-called negative mobility behavior has been observed in highly spatially inhomogeneous materials [17, 18].

Often when interpreting experimental mobility results in organic and disordered materials, it is found that no theory adequately explains various transport phenomena, particularly the electric field and temperature dependencies of drift mobility [19–23]. In particular, the most frequently used approaches refer to hopping transport character in disordered organic solids and are based either on a modified Poole-Frenkel (PF) model [20] or a Gaussian disorder model (GDM) [24]. In the Poole-Frenkel model the mobility can be described as a field and temperature assisted detrapping process of a carrier from the Coulomb potential

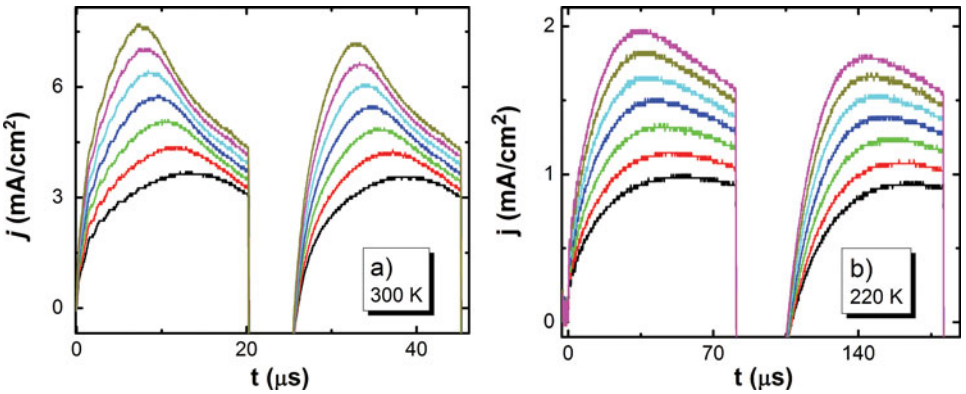

Figure 6. Examples of the characteristic CELIV traces at 300 K (a) and 220 K (b).

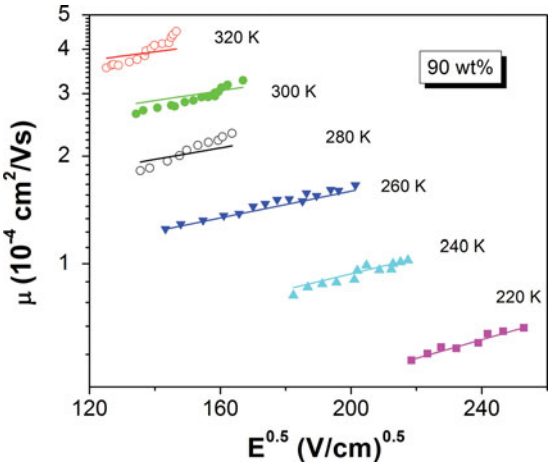

Figure 7. Mobility dependencies on the applied electric field in the sample with 90 wt% of NCs at different temperatures. Solid lines represent fitting according to the Gaussian Disorder Model.

of a charged trap. While the Poole-Frenkel model describes both the mobility increase with electric field strength as well as its decrease, it does not provide any physical clues about the nature of the processes. In contrast, in the GDM model, transport is driven by charge hopping within a Gaussian distribution of site energies. The density of states reflects the energetic spread in the charge transporting levels of chain segments due to fluctuation in conjugation lengths and structural disorder. Within the Gaussian disorder model the mobility is given by [24]:

$$\mu(F,T) = \mu_\infty \exp\left[-\left(\frac{2\sigma}{3kT}\right)^2\right] \exp\left\{C\left[\left(\frac{\sigma}{kT}\right)^2 - \Sigma^2\right]\sqrt{F}\right\}. \quad (5)$$

This equation was derived from Monte-Carlo simulations of the hopping processes of charge carriers in a material with energetic (σ) and positional disorder (Σ) described be Gaussian distribution functions. μ_∞. is the high temperature limit of the mobility and C is a positive numerical factor ($C = 2.9 \times 10^{-4}$ (cm/V)$^{1/2}$ from the simulations that originally led to the formulation of the GDM). Here we used the GDM model to fit the experimental data, as shown in Fig. 7 for the case of the 90 wt% sample. The experimental $\mu(T)$ curves obtained for each sample were fitted with a single set of parameters, given in Table 2.

Table 2. Fit parameters for the Gaussian Disorder Modeling of the mobility data, for hybrid blends with various NC weight ratios

	90 wt%	83 wt%	75 wt%	50 wt%
μ_∞(cm^2/Vs)	4.75×10^{-3}	8×10^{-3}	1.30×10^{-2}	1.1×10^{-3}
Σ	1.5	2	2	2.4
σ (eV)	0.071	0.08	0.08	0.07
C (cm/V)$^{0.5}$	3.5×10^{-4}	2×10^{-4}	4.00×10^{-4}	3.8×10^{-4}

From Table 2 it can be seen that the best charge transport conditions are achieved in the samples with 75 wt% and 85 wt% of the NCs. First, these samples exhibit high mobilities μ_∞ values. Second, the values of the energetical disorder parameter σ are the highest, indicating higher potential barriers existing in the system. Meanwhile parameter of the spatial disorder $\sum$ is intermediate: not too high to prevent carrier jumps from site to site, and not too low to limit recombination. On the other hand the value of the spatial disorder parameter $\sum$ is relatively small indicating that spatial heterostructure is not well expressed.

Summary and Conclusions

Electrical charge transport properties of hybrid test structures made of P3HT and branched CdSe NCs were investigated. The NCs were branched, with average arm and core diameters of 3.8 nm and average arm length of 6.3 nm. To evaluate the impact of the NCs content in the blend on the device performance, we screened different weight proportions from 50 wt% (16 vol%) to 90 wt% (63 vol%). We utilized the Charge Extraction by Linear Increasing Voltage (CELIV) and temperature dependent conductivity measurements to analyse the charge mobility, energetical and positional disorder parameters, and activation energy. The photovoltaic phenomenon was observed in the samples with content of NCs above 75 wt%. The samples with 50 wt% were photoconductive, but no PV effect could be observed, probably because of the inefficient exciton dissociation at the reduced donor-acceptor interface and because of the absence of efficient percolation pathways. The thermal activation energy of carrier generation in the dark was evaluated to be 0.14–0.18 eV; it decreased upon illumination for the samples showing no PV effect and increased in the films exhibiting photovoltaic behavior. In the samples with content of NCs above 75 wt%, Open Circuit Voltages up to 1 V were obtained. Nevertheless fast recombination of the generated carriers was pronounced and could be limiting factor of the cell current. Carrier mobility at room temperature was about $(3-4) \times 10^{-4}$ cm^2/Vs in the samples with 75 wt% and 83 wt% of NCs, which is higher than the one measured in pure P3HT. The Gaussian Disorder Model was used to describe the variations of the mobilities with the applied electric field strength and the temperature. This showed that the transport is optimal in the samples with 75 wt% and 83 wt% of NCs, as was observed by Time-of-Flight mobility measurements in similar samples [11].

Funding

The partial financial support from the Research Council of Lithuania (Project No TAP LZ 01/2013) and EGIDE agency of France within the Gilibert Programme is acknowledged. E. C. PhD grant was supported by the Commissariat à l'Énergie Atomique et aux Énergies Alternatives.

References

[1] Reiss, P., Couderc, E., De Girolamo, J., & Pron, A. (2011). *Nanoscale*, *3*, 446.
[2] Ren, S., Chang, L.-Y., Lim, S.-K., Zhao, J., Smith, M., Zhao, N., Bulovici, V., Bawendi, M., & Gradecak, S. (2011). *Nano Lett.*, *11*, 3998.
[3] Zhou, R., Stadler, R., Xie, D., Cao, W., Zheng, Y., Yang, Y., Plaisant, M., Holloway, P. H., Schanze, K. S., Reynolds, J. R., & Xue, J. (2013). *ACS Nano*, *7*, 4846.
[4] Kuo, C.-Y., Su, M.-S., Chen, G.-Y., Ku, C.-S., Lee, H.-Y., & Wei, K.-H. (2011). *Energy & Environmental Science*, *4*, 2316.

[5] Greaney, M. J., Araujo, J., Burkhart, B., Thompson, B. C., & Brutchey, R. L. (2013). *Chem. Commun.*, *49*, 8602–8604.
[6] Peet, J., Kim, J. Y., Coates, N. E., Ma, W. L., Moses, D., Heeger, A. J., & Bazan, G. C. (2007). *Nature Mater.*, *6*, 497.
[7] Chen, G.-Y., Cheng, Y.-H., Chou, Y.-J., Su, M.-S., Chen, C.-M., & Wei, K.-H. (2011). *Chem. Commun.*, *47*, 5064.
[8] Ma, W., Yang, C., Gong, X., Lee, K., & Heeger, A. J. (2005). *Adv. Funct. Mater.*, *15*, 1617.
[9] Yang, J., Tang, A., Zhou, R., & Xue, J. (2011). *Sol. Energy Mater. Sol. Cells*, *95*, 476.
[10] Dayal, S., Reese, M. O., Ferguson, A. J., Ginley, D. S., Rumbles, G., & Kopidakis, N. (2010). *Adv. Funct. Mater.*, *20*, 2629.
[11] Couderc, E., Bruyant, N., Fiore, A., Chandezon, F., Djurado, D., Reiss, P., & Faure-Vincent, J. (2012). *Appl. Phys. Lett.*, *101*, 133301.
[12] Riess, W. (1997). In: *Organic electroluminescent materials and devices*. Eds. S. Miyata and H. S. Nalva. Gordon and Breach, Amsterdam, pp. 73–146.
[13] Godlewski, J. & Kalinowski, J. (1989). *Jap. J. Appl. Phys.*, *28*, 24.
[14] Nelson, J., Kirkpatrick, J., & Ravirajan, P. (2004). *Phys. Rev. B*, *69*, 035337.
[15] Kažukauskas, V., Arlauskas, A., Pranaitis, M., Lessmann, R., Riede, M., & Leo, K. (2010). *Opt. Mater.*, *32*, 1676.
[16] Kažukauskas, V., Arlauskas, A., Pranaitis, M., Glatthaar, M., & Hinsch, A. (2010). *J. Nanosci. Nanotechnol.*, *10*, 1376.
[17] Kažukauskas, V., Pranaitis, M., Sicot, L., & Kajzar, F. (2006). *Mol. Cryst. Liq. Cryst.*, *447*, 459.
[18] Mozer, A. J., Sariciftci, N. S., Pivrikas, A., Österbacka, R., Juška, G., Brassat, L., & Bässler, H. (2005). *Phys. Rev. B*, *71*, 035214.
[19] Kepler, R. G., Beeson, P. M., Jacobs, S. J., Anderson, R. A., Sinclair, M. B., Valencia, V. S., & Cahill, P. A. (1995). *Appl. Phys. Lett.*, *66*, 3618.
[20] Gill, W. D. (1972). *Appl. Phys.*, *43*, 5033.
[21] Abkowitz, M. A. (1992). *Philos. Mag. B*, *65*, 817.
[22] Schein, L. B. (1992). *Philos. Mag. B*, *65*, 795.
[23] Blom, P. W. M. & Vissenberg, M. C. J. M. *Mater. Sci. Eng.*, *27*, 53.
[24] Baessler, H. (1993). *Phys. Stat. Solidi (b)*, *175*, 15.